Journal of
Mechanics of
Materials and Structures

MICROMECHANICAL STUDY OF DISPERSION AND DAMPING CHARACTERISTICS OF GRANULAR MATERIALS

Niels P. Kruyt

Volume 7, No. 4 April 2012

mathematical sciences publishers

JOURNAL OF MECHANICS OF MATERIALS AND STRUCTURES
Vol. 7, No. 4, 2012

MICROMECHANICAL STUDY OF DISPERSION AND DAMPING CHARACTERISTICS OF GRANULAR MATERIALS

NIELS P. KRUYT

The wave-propagation characteristics of dense granular materials have been studied from the micromechanical viewpoint, in which relationships are sought between properties at the micro-scale of particles and interparticle contacts and properties at the continuum, macro-scale. The dispersion and damping characteristics have been determined from a three-dimensional lattice analysis in which the particle interaction is modeled with linear elastic springs and linear viscous dashpots.

Due the presence of rotational degrees of freedom of the particles, optical branches are observed in the dispersion and damping characteristics, besides the acoustical branches. The influence of the micromechanical characteristics on the macroscopic dispersion and damping characteristics has been determined for a face-centered cubic lattice and a body-centered cubic lattice. For small wave numbers (large wave lengths) the damping of the optical branches is very large. This means that the optical branches will not be observed in conditions where a continuum-mechanical description is appropriate.

1. Introduction

In many disciplines of engineering, the propagation of waves is important. For example, wave propagation in granular materials is important in oil exploration. Granular materials are special materials in the sense that they possess a clear, discrete structure of particles with rotational degrees of freedom and interparticle contacts. In micromechanics of granular materials, relationships are investigated between properties at the micro-scale of particles and interparticle contacts and properties at the continuum, macro-scale.

Here the characteristics of wave propagation, dispersion and damping, are studied from the micromechanical viewpoint. In this approach the three-dimensional granular assembly is modeled as a large set of spherical particles that only interact at contacts through linear elastic springs and linear viscous dampers in directions normal and tangential to contacts.

The focus is on isotropic, dense or cemented granular materials where the particle displacements are small and the number of interparticle contacts does not change. Particle dampers (see for example [Els 2011]), where damping through particle collisions is important, are not considered.

The wave-propagation characteristics consist of the dispersion and damping characteristics. These characteristics give the complex circular frequencies $\omega = \omega(\boldsymbol{k})$ that are compatible with plane-wave solutions of the governing equations with a periodic spatial variation that is characterized by the wave vector $\boldsymbol{k}$, i.e., solutions for the unknowns $\boldsymbol{u}$ of the form

$$\begin{aligned}\boldsymbol{u}(\boldsymbol{x}, t) &= \boldsymbol{V} \exp[j(\omega t - \boldsymbol{k}\cdot\boldsymbol{x})] \\ &= \boldsymbol{V} \exp[-j\boldsymbol{k}\cdot\boldsymbol{x}] \exp[j\mathrm{Re}(\omega)t] \exp[-\mathrm{Im}(\omega)t],\end{aligned} \tag{1-1}$$

Keywords: wave propagation, granular materials, dispersion, damping.

where $\boldsymbol{x}$ is the position vector, t is time, j is the imaginary unit, $\boldsymbol{V}$ is an amplitude vector, $\mathrm{Re}(\omega)$ and $\mathrm{Im}(\omega)$ are the real part and the imaginary part of the complex circular frequency, respectively. The dispersion characteristics are given by $\mathrm{Re}(\omega)$ and the damping characteristics by $\mathrm{Im}(\omega)$. Note that $\mathrm{Im}(\omega) > 0$ for actual damping (reduction of the amplitude of $\boldsymbol{u}$ with time t).

The magnitude of the wave vector $\boldsymbol{k}$ is the wave number k. The wave number k is related to the wave length Λ by

$$\Lambda = \frac{2\pi}{k}. \tag{1-2}$$

Wave speeds for small wave numbers (large wave lengths) have been studied experimentally (see for example [Jia et al. 1999] and the references given in [Magnanimo et al. 2008]), theoretically (for example [Goddard 1990]), and numerically (for example [Makse et al. 2004; Agnolin and Roux 2007; Mouraille 2009]), showing a clear dependence on confining pressure. The pressure dependence is not studied here. This dependence can be incorporated by a proper choice for the dependence of the micromechanical parameters (interparticle stiffnesses and the coordination number, i.e., the average number of contacts per particle, as described in detail in Section 3) on confining pressure.

Suiker et al. [2001] and Suiker and de Borst [2005] derived dispersion relations for granular materials, based on a two-dimensional elastic lattice model of granular material (without damping). Schwartz et al. [1984] considered the dispersion relation of a three-dimensional face-centered cubic elastic lattice (FCC lattice for short), while Kruyt [2010] studied the dispersion relation for general three-dimensional elastic lattices (including the FCC lattice studied in [Schwartz et al. 1984]) and determined the influence of the micromechanical parameters on the dispersion characteristics. In all these lattice models the rotational degrees of freedom are explicitly accounted for. This leads to the presence of so-called optical branches in the dispersion relation, with nonzero circular frequency ω for small wave number k. Such optical branches also arise in solid state physics (see for example [Kittel 1953; Dekker 1962; Ashcroft and Mermin 1976; Myers 1997]) in the presence of atoms with varying properties, where the optical branches correspond to movement of the atoms relative to that of the center of mass of the unit cell.

Previous analyses are extended here by also taking viscous damping into account in the micromechanical model. Thus, dispersion *and* damping characteristics are obtained here, in terms of particle and interparticle characteristics, using three-dimensional lattice-based approaches. These results will be used to investigate what the (regularising) influence is of (small) viscous damping at the micro-scale on the macro-scale damping of the optical branches with their high circular frequencies for small wave number.

The outline of this study is as follows. Firstly, (classical) continuum-mechanical dispersion and damping characteristics are formulated for a viscoelastic material model in Section 2 in order to establish the continuum-mechanical framework. The relevant micromechanics of granular materials is described in Section 3. This is followed by the three-dimensional lattice formulation in Section 4. Results for the dispersion and damping characteristics are given in Section 5. Finally, findings from this study are summarized in Section 6.

2. Continuum-mechanical dispersion and damping characteristics

Dispersion characteristics for elastic materials are derived in many textbooks, based on classical continuum mechanics. For extended continua, such as Cosserat continua and micropolar continua that

incorporate couple stresses and (independent) rotational degrees of freedom, respectively, such dispersion characteristics for purely elastic materials have also been obtained [Eringen 1999].

For a viscoelastic material the continuum-mechanical dispersion and damping characteristics are analysed here, based on classical continuum mechanics. For small deformations $\boldsymbol{u}$ the governing conservation equation of momentum is

$$\rho \ddot{\boldsymbol{u}} = \nabla \cdot \boldsymbol{\sigma}, \tag{2-1}$$

where ρ is the density, the two superimposed dots denote the second derivative of $\boldsymbol{u}$ with respect to time t and $\boldsymbol{\sigma}$ is the stress increment (with respect to an equilibrium state). The stress increment is described by a (Kelvin–Voigt) viscoelastic model

$$\boldsymbol{\sigma} = \{\lambda \operatorname{tr}(\boldsymbol{\epsilon})\boldsymbol{I} + 2G\boldsymbol{\epsilon}\} + \{\kappa \operatorname{tr}(\dot{\boldsymbol{\epsilon}})\boldsymbol{I} + 2\eta\dot{\boldsymbol{\epsilon}}\}, \tag{2-2}$$

with the strain increment tensor $\boldsymbol{\epsilon}$ given by

$$\boldsymbol{\epsilon} = \tfrac{1}{2}[\nabla \boldsymbol{u} + (\nabla \boldsymbol{u})^T]. \tag{2-3}$$

The parameters λ and G are the elastic Lamé constants and the parameters κ and η are corresponding viscosities. The parameter λ is related to the bulk modulus K by

$$K = \lambda + \tfrac{2}{3}G. \tag{2-4}$$

With a plane-wave solution for the displacement vector $\boldsymbol{u}$ according to (1-1), it follows from (2-1), (2-2) and (2-3), after some algebra, that the circular frequency ω must satisfy the following quadratic eigenvalue problem

$$[\{(\lambda + j\kappa\omega) + (G + j\eta\omega)\}\boldsymbol{k}\boldsymbol{k} + (G + j\eta\omega)k^2\boldsymbol{I}] \cdot \boldsymbol{V} - \rho\omega^2\boldsymbol{V} = \boldsymbol{0}, \tag{2-5}$$

where $\boldsymbol{I}$ is the 3-by-3 identity matrix.

After some further algebra we find the solutions:

- a *longitudinal branch* where the eigenvector $\boldsymbol{V}$ is in the direction of the wave vector $\boldsymbol{k}$:

$$\operatorname{Re}(\omega) \cong \sqrt{\frac{\lambda+2G}{\rho}}k, \quad \operatorname{Im}(\omega) \cong \frac{\kappa+2\eta}{2\rho}k^2; \tag{2-6}$$

- a *transverse branch* where the eigenvector $\boldsymbol{V}$ is perpendicular to the wave vector $\boldsymbol{k}$:

$$\operatorname{Re}(\omega) \cong \sqrt{\frac{G}{\rho}}k, \quad \operatorname{Im}(\omega) \cong \frac{\eta}{2\rho}k^2. \tag{2-7}$$

The multiplicity of the eigenvalue of the longitudinal branch equals one, while that of the transverse branch equals two. The longitudinal and transverse branches are called *acoustical*, as the dispersion characteristics $\operatorname{Re}(\omega)$ are proportional to the wave number k and hence cross the origin (contrary to the *optical* branches). Their damping characteristics $\operatorname{Im}(\omega)$ are proportional to k^2.

This continuum-mechanical approach is valid in the large wave-length case, that is, for small wave number k.

3. Micromechanics

Three-dimensional assemblies consisting of spherical particles are considered here. The radius of particle p is denoted by R^p and the position of the center of mass of particle p is given by $\boldsymbol{X}^p$. For two particles p and q in contact, $\boldsymbol{r}^{pq}$ is the vector directed from the center of particle p to the contact point between particles p and q, with an analogous definition for $\boldsymbol{r}^{qp}$. For very stiff particles where the "overlap" (elastic deformation) at contacts is small, the unit normal vector $\boldsymbol{n}^{pq}$ at the contact is obtained from

$$\boldsymbol{r}^{pq} = R^p \boldsymbol{n}^{pq}. \tag{3-1}$$

The direction of the normal vector $\boldsymbol{n}^{pq}$ determines the orientation of the contact.

The (small) displacement vector of the center of particle p, relative to the selected reference equilibrium configuration, is denoted by $\boldsymbol{u}^p$, while the (small) particle rotation vector is indicated by $\boldsymbol{\theta}^p$. The equations of motion governing the evolution with time t of the displacement $\boldsymbol{u}^p$ and rotation $\boldsymbol{\theta}^p$ of the spherical particle p are

$$m^p \ddot{\boldsymbol{u}}^p = \sum_q \boldsymbol{f}^{pq}, \quad I^p \ddot{\boldsymbol{\theta}}^p = \sum_q \boldsymbol{r}^{pq} \times \boldsymbol{f}^{pq}, \tag{3-2}$$

where the two superimposed dots denote the second derivative of the quantity involved with respect to time t, m^p and I^p are the mass and moment of inertia of the particle p, respectively, $\boldsymbol{f}^{pq}$ is the force exerted on particle p by particle q and the sum is over particles q that are in contact with particle p. The moment of inertia I^p for a sphere with radius R^p and mass m^p is given by

$$I^p = Q m^p {R^p}^2, \tag{3-3}$$

where $Q = \frac{2}{5}$ for a solid sphere and $Q = \frac{2}{3}$ for a hollow sphere. In the following, solid spheres with $Q = \frac{2}{5}$ are considered when numerical results are presented. Note that body forces, like gravitational forces, have been excluded in (3-2).

The relative displacement vector $\boldsymbol{\Delta}^{pq}$ at the contact point between two particles in contact p and q is given by

$$\boldsymbol{\Delta}^{pq} = [\boldsymbol{u}^p + \boldsymbol{\theta}^p \times \boldsymbol{r}^{pq}] - [\boldsymbol{u}^q + \boldsymbol{\theta}^q \times \boldsymbol{r}^{qp}]. \tag{3-4}$$

Note that the relative displacement vector involves contributions due to particle translations $\boldsymbol{u}^p$ and due to particle rotations $\boldsymbol{\theta}^p$.

The (increment of the) contact force $\boldsymbol{f}^c$ at contact c is related to the relative displacement $\boldsymbol{\Delta}^c$ and the relative velocity $\dot{\boldsymbol{\Delta}}^c$ (i.e., the time derivative of the relative displacement) at the contact through the contact constitutive relation. Since small displacements are considered, the contact constitutive relation can be formulated in a linearized form that considers two mechanisms: elastic deformation and viscous damping.

Coulomb frictional damping is not considered here, since the focus is on isotropic states where the number of contacts where Coulomb friction is fully mobilized is small. Because of the assumption of small displacements, contacts that are in an elastic state will remain to do so.

Hertz–Mindlin theory (see for example [Johnson 1985]) gives a nonlinear dependence of the elastic interparticle forces on the relative displacements. In the adopted small-displacement approach, the linearized form of this relation is described by two (linear) elastic springs in normal and tangential directions

at the contact, with spring stiffnesses k_n and k_t, respectively. The spring stiffnesses k_n and k_t then depend on the normal force in the equilibrium state, and hence on the (average) confining pressure.

As with the elastic interaction, the relation between the viscous force and the relative velocity is described by two linear viscous dashpots in normal and tangential directions at the contact, with viscous damping coefficients d_n and d_t, respectively.

The employed contact constitutive relation then can be written as

$$\boldsymbol{f}^c = -\boldsymbol{S}^c \cdot \boldsymbol{\Delta}^c - \boldsymbol{D}^c \cdot \dot{\boldsymbol{\Delta}}^c, \tag{3-5}$$

where the (elastic) contact stiffness matrix $\boldsymbol{S}^c$ and the (viscous) contact damping matrix $\boldsymbol{D}^c$ are given by

$$\boldsymbol{S}^c = (k_n - k_t)\boldsymbol{n}^c\boldsymbol{n}^c + k_t\boldsymbol{I}, \quad \boldsymbol{D}^c = (d_n - d_t)\boldsymbol{n}^c\boldsymbol{n}^c + d_t\boldsymbol{I}. \tag{3-6}$$

Here $\boldsymbol{I}$ is the 3-by-3 identity matrix. Note that these expressions satisfy Newton's third law, $\boldsymbol{f}^{qp} = -\boldsymbol{f}^{pq}$, since $\boldsymbol{\Delta}^{qp} = -\boldsymbol{\Delta}^{pq}$ and the contact stiffness and damping matrices are symmetrical.

The normal and tangential viscous damping coefficients, d_n and d_t, can also be expressed in terms of normal and tangential coefficients of restitution [Wu et al. 2003; Kruggel-Emden et al. 2007; Schwager and Pöschel 2007; Schwager et al. 2008; O'Sullivan 2011].

The equations of motion, Equations (3-2), can be expressed concisely in terms of a generalized displacement vector $\boldsymbol{U}^p$, a generalized force vector $\boldsymbol{F}^{pq}$ and a generalized mass matrix $\boldsymbol{M}^p$ by

$$\boldsymbol{M}^p \cdot \ddot{\boldsymbol{U}}^p = \sum_q \boldsymbol{F}^{pq}, \quad \boldsymbol{U}^p = \begin{bmatrix} \boldsymbol{u}^p \\ R^p\boldsymbol{\theta}^p \end{bmatrix}, \quad \boldsymbol{M}^p = m^p \begin{bmatrix} \boldsymbol{I} & \boldsymbol{0} \\ \boldsymbol{0} & Q\boldsymbol{I} \end{bmatrix}, \quad \boldsymbol{F}^{pq} = \begin{bmatrix} \boldsymbol{f}^{pq} \\ \boldsymbol{n}^{pq} \times \boldsymbol{f}^{pq} \end{bmatrix}. \tag{3-7}$$

Note that the terms in $\boldsymbol{U}^p$ and $\boldsymbol{F}^{pq}$ have the same dimension (or unit), through the inclusion and exclusion, respectively, of the particle radius R^p. For compactness in notation, the generalized force $\boldsymbol{F}^{pq}$ is expressed as

$$\boldsymbol{F}^{pq} = \begin{bmatrix} \boldsymbol{I} \\ \boldsymbol{N}^{\times pq} \end{bmatrix} \cdot \boldsymbol{f}^{pq}, \tag{3-8}$$

where the operator $\boldsymbol{N}^{\times pq}$ is defined by the equality $\boldsymbol{N}^{\times pq} \cdot \boldsymbol{v} = \boldsymbol{n}^{pq} \times \boldsymbol{v}$ for all $\boldsymbol{v}$. Thus

$$\boldsymbol{N}^{\times pq} = -\boldsymbol{P} \cdot \boldsymbol{n}^{pq}, \tag{3-9}$$

with $\boldsymbol{P}$ the three-dimensional permutation symbol.

4. Lattice formulation

The regular lattice geometry is described as follows (see Figure 1). A central particle '0' at position $\boldsymbol{X}_0$ is in contact with Z other particles. All particles have the same properties, such as identical particle radius R, mass m and coordination number Z, i.e., the number of contacts per particle. The unit normal vector at the contact c is denoted by $\boldsymbol{n}^c$. The set of normal vectors $\{\boldsymbol{n}^c\}$ determines the lattice directions. The position of the center $\boldsymbol{X}^c$ of the other particles in contact with the central particle '0' is given by $\boldsymbol{X}^c = \boldsymbol{X}_0 + 2R\boldsymbol{n}^c$. Two different three-dimensional lattices will be considered in detail in the following. These are the face-centered cubic (FCC) and body-centered cubic (BCC) lattices, as shown in Figure 2. The fabric tensor [Horne 1965], based on the contact normals, is isotropic for these lattices.

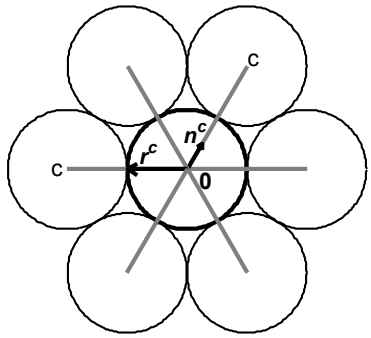

Figure 1. Example of a two-dimensional lattice with coordination number $Z = 6$. Also indicated are the contact normal vector $\boldsymbol{n}^c$ and the vector $\boldsymbol{r}^c$ from the center of the particle to the point of contact.

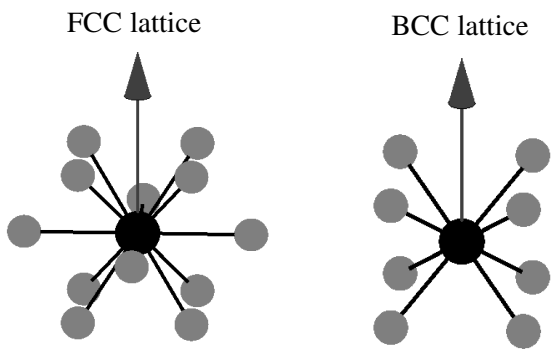

Figure 2. Lattice geometry. Left: FCC lattice, with coordination number $Z = 12$. Right: BCC lattice, with coordination number $Z = 8$. The central sphere of each lattice is shown in black, while the other spheres that are in contact with the central one are shown in gray. The radius of the spheres has been reduced for visual clarity: therefore the spheres in contact appear as if they were not in contact. Contacts between spheres are indicated by black lines connecting particle centers. The direction of the wave vector is indicated by the upward arrow.

For the *spatial* variation of the generalized displacement vector $\boldsymbol{U}(\boldsymbol{x}, t)$, a periodic variation is assumed

$$\boldsymbol{U}(\boldsymbol{x}, t) = \boldsymbol{U}_0(t) \exp[-j\boldsymbol{k} \cdot (\boldsymbol{x} - \boldsymbol{X}_0)] = \begin{bmatrix} \boldsymbol{u}_0(t) \\ R\boldsymbol{\theta}_0(t) \end{bmatrix} \exp[-j\boldsymbol{k} \cdot (\boldsymbol{x} - \boldsymbol{X}_0)], \tag{4-1}$$

where $\boldsymbol{u}_0(t)$ and $\boldsymbol{\theta}_0(t)$ are the time-dependent amplitude vectors for the displacements and rotations, respectively.

Employing the assumed solution according to (4-1), the relative displacement vector $\boldsymbol{\Delta}^c$ at contact c becomes, from (3-4) with $\boldsymbol{r}^{0c} = R\boldsymbol{n}^c$ and $\boldsymbol{r}^{c0} = -R\boldsymbol{n}^c$ for spherical particles with equal radius R,

$$\boldsymbol{\Delta}^c = (1 - \xi^c)\boldsymbol{u}_0 + (1 + \xi^c)R\boldsymbol{\theta}_0 \times \boldsymbol{n}^c, \quad \xi^c = \exp[-j(2R)\boldsymbol{k} \cdot \boldsymbol{n}^c]. \tag{4-2}$$

Note that the scalar factor ξ^c (also) depends on the wave vector $\boldsymbol{k}$. The relative displacement vector can be expressed in terms of the amplitude vector $\boldsymbol{U}_0$ and the operator $\boldsymbol{N}^{\times c}$ defined in (3-9) by

$$\boldsymbol{\Delta}^c = \left[(1-\xi^c)\boldsymbol{I} \quad -(1+\xi^c)\boldsymbol{N}^{\times c}\right] \cdot \boldsymbol{U}_0, \tag{4-3}$$

where the term inside the square brackets is a 3 by 6 matrix, which does not involve a subtraction.

It then follows that the amplitude vector $\boldsymbol{U}_0$ satisfies the second-order ordinary differential equation

$$\boldsymbol{M} \cdot \ddot{\boldsymbol{U}}_0 + \bar{\boldsymbol{D}} \cdot \dot{\boldsymbol{U}}_0 + \bar{\boldsymbol{K}} \cdot \boldsymbol{U}_0 = \boldsymbol{0}, \tag{4-4}$$

where the effective damping matrix $\bar{\boldsymbol{D}}$ and the effective stiffness matrix $\bar{\boldsymbol{K}}$ are given by

$$\begin{aligned} \bar{\boldsymbol{D}} &= \sum_{c=1}^{C} \begin{bmatrix} \boldsymbol{I} \\ \boldsymbol{N}^{\times c} \end{bmatrix} \cdot \boldsymbol{D}^c \cdot \left[(1-\xi^c)\boldsymbol{I} \quad -(1+\xi^c)\boldsymbol{N}^{\times c}\right], \\ \bar{\boldsymbol{K}} &= \sum_{c=1}^{C} \begin{bmatrix} \boldsymbol{I} \\ \boldsymbol{N}^{\times c} \end{bmatrix} \cdot \boldsymbol{S}^c \cdot \left[(1-\xi^c)\boldsymbol{I} \quad -(1+\xi^c)\boldsymbol{N}^{\times c}\right]. \end{aligned} \tag{4-5}$$

The size of the matrices $\bar{\boldsymbol{D}}$ and $\bar{\boldsymbol{K}}$ is 6 by 6. It can be shown, after some algebra, that the matrices $\bar{\boldsymbol{D}}$ and $\bar{\boldsymbol{K}}$ are Hermitian, using the fact that for every lattice direction $\boldsymbol{n}^c$ there is a corresponding direction $-\boldsymbol{n}^c$, $\boldsymbol{S}(-\boldsymbol{n}^c) = \boldsymbol{S}(\boldsymbol{n}^c)$, $\boldsymbol{D}(-\boldsymbol{n}^c) = \boldsymbol{D}(\boldsymbol{n}^c)$, $\boldsymbol{N}^{\times}(-\boldsymbol{n}^c) = -\boldsymbol{N}^{\times}(\boldsymbol{n}^c)$ and $\xi(-\boldsymbol{n}^c) = \xi^*(\boldsymbol{n}^c)$. Here ξ^* denotes the complex conjugate of ξ.

For an harmonic variation in time for the amplitude vector $\boldsymbol{U}_0(t)$

$$\boldsymbol{U}_0(t) = \boldsymbol{U}_a \exp j\omega t, \tag{4-6}$$

we obtain the following *quadratic eigenvalue problem* for the (complex) eigenfrequencies $\omega = \omega(\boldsymbol{k})$

$$[-\omega^2 \boldsymbol{M} + j\omega\bar{\boldsymbol{D}} + \bar{\boldsymbol{K}}] \cdot \boldsymbol{U}_a = \boldsymbol{0}. \tag{4-7}$$

The eigenfrequencies of this quadratic eigenvalue problem can be computed numerically from (4-7) or they can be obtained from the solution of a (larger) generalized eigenvalue problem that is obtained from the so-called linearisation approach (see for example, [Tisseur and Meerbergen 2001]). When considering analytical solutions, it is more convenient to consider the generalized eigenvalue problem. The linearisation approach is outlined in the next Section.

4A. ***Linearisation approach.*** The system (4-4) of second-order equations of motion can be rewritten as a larger system of first-order ordinary differential equations by introducing the variable (see for example [Tisseur and Meerbergen 2001])

$$\boldsymbol{P}_0 = \begin{bmatrix} \dot{\boldsymbol{U}}_0 \\ \boldsymbol{U}_0 \end{bmatrix}. \tag{4-8}$$

The resulting system of first-order ordinary differential equations is

$$\begin{bmatrix} \boldsymbol{M} & \boldsymbol{0} \\ \boldsymbol{0} & \hat{\boldsymbol{I}} \end{bmatrix} \cdot \dot{\boldsymbol{P}}_0 + \begin{bmatrix} \bar{\boldsymbol{D}} & \bar{\boldsymbol{K}} \\ -\hat{\boldsymbol{I}} & \boldsymbol{0} \end{bmatrix} \cdot \boldsymbol{P}_0 = \boldsymbol{0}, \tag{4-9}$$

where $\hat{\boldsymbol{I}}$ is the 6 by 6 identity matrix. With an harmonic time-dependence of $\boldsymbol{P}_0(t) = \boldsymbol{P}_a \exp[j\omega t]$, a generalized eigenvalue problem is obtained for the circular frequency ω

$$\begin{bmatrix} \bar{\boldsymbol{D}} & \bar{\boldsymbol{K}} \\ -\hat{\boldsymbol{I}} & \boldsymbol{0} \end{bmatrix} \cdot \boldsymbol{P}_a = \omega(-j) \begin{bmatrix} \boldsymbol{M} & \boldsymbol{0} \\ \boldsymbol{0} & \hat{\boldsymbol{I}} \end{bmatrix} \cdot \boldsymbol{P}_a. \tag{4-10}$$

4B. ***Branches in the dispersion and damping characteristics.*** From the numerical results for the eigenvectors corresponding to the eigenfrequencies, the dominant mode of motion has been identified for each eigenfrequency. This leads to the distinction of the following branches in the dispersion and damping characteristics (see also Section 2):

LA (longitudinal acoustical): the dominant motion is *longitudinal displacement*, i.e., in the direction of the wave vector $\boldsymbol{k}$; the multiplicity of the eigenfrequency is one;

TA (transverse acoustical): the dominant motion is *transverse displacement*, relative to the direction of the wave vector $\boldsymbol{k}$; the multiplicity of the eigenfrequency is two;

LO (longitudinal optical): the dominant motion is *longitudinal rotation*, i.e., in the direction of the wave vector $\boldsymbol{k}$; the multiplicity of the eigenfrequency is one;

TO (transverse optical): the dominant motion is *transverse rotation*, relative to in the direction of the wave vector $\boldsymbol{k}$; the multiplicity of the eigenfrequency is two.

The acoustical branches also resulted from the classical continuum-mechanical analysis of Section 2. Extended continuum-mechanical theories (see for example, [Mindlin 1972; Kunin 1982; 1983; Eringen 1999; Suiker et al. 2001; Suiker and de Borst 2005]) also give optical branches in the dispersion characteristics. In the lattice-based micromechanical analysis the optical branches arise due to the presence of rotational degrees of freedom [Schwartz et al. 1984; Suiker et al. 2001; Suiker and de Borst 2005; Kruyt 2010].

For future reference, non-dimensional micromechanical parameters are introduced that relate

(1) the tangential elastic stiffness to the normal elastic stiffness,

(2) the tangential viscous damping coefficient to the normal viscous damping coefficient and

(3) the normal viscous damping coefficient to the normal elastic stiffness and the particle mass.

The stiffness ratio r_K, the damping ratio r_D and the damping factor ζ (often called the damping ratio) are defined by

$$r_K = \frac{k_t}{k_n}, \quad r_D = \frac{d_t}{d_n}, \quad \zeta = \frac{d_n}{2\sqrt{k_n m}}. \tag{4-11}$$

The nondimensional wave number $\hat{k}$ and nondimensional frequency $\hat{\omega}$ are defined by

$$\hat{k} = \left(\frac{2R}{\pi}\right)k, \quad \hat{\omega} = \sqrt{\frac{m}{k_n}}\omega. \tag{4-12}$$

4C. ***Analytical solution for FCC lattice for small wave number.*** For small wave number k, analytical solutions for the eigenfrequencies ω have been found by factoring the characteristic polynomial corresponding to (4-10). From a Taylor expansion in wave number k, the solutions for an FCC lattice are obtained after some lengthy algebra (using a symbolic mathematics package). The results for the

non-dimensional real and the imaginary parts of the non-dimensional eigenfrequencies $\hat{\omega}$ are given in Table 1.

Longitudinal	$\mathrm{Re}(\hat{\omega}) \cong 2\sqrt{1+r_K}(Rk)$	$\mathrm{Im}(\hat{\omega}) \cong 4(1+4r_D)\zeta(Rk)^2$
Transverse	$\mathrm{Re}(\hat{\omega}) \cong \sqrt{2}\sqrt{1+r_K}(Rk)$	$\mathrm{Im}(\hat{\omega}) \cong 2(1+r_D)\zeta(Rk)^2$
Optical	$\mathrm{Re}(\hat{\omega}) \cong \frac{4}{Q}\sqrt{Qr_K - 16r_D^2\zeta^2}$	$\mathrm{Im}(\hat{\omega}) \cong \frac{16r_D\zeta}{Q}$

Table 1. Real and imaginary parts of the nondimensional eigenfrequencies $\hat{\omega}$ in the three situations considered.

The multiplicity of the eigenfrequency for the longitudinal branch equals one, that for the transverse equals two and for the optical branch three (both longitudinal and transverse optical).

The dispersion characteristics show branches where $\mathrm{Re}(\omega)$ is proportional to k and the damping characteristics show branches where $\mathrm{Im}(\omega)$ is proportional to k^2. These results are consistent with the results of the classical continuum-mechanical analysis of Section 2 that is based on a viscoelastic continuum material model.

The reduction in time t of the *amplitude* of the generalized displacement vector $\boldsymbol{U}$ is given by

$$\frac{\|\boldsymbol{U}(\boldsymbol{x},t)\|}{\|\boldsymbol{U}(\boldsymbol{x},0)\|} = e^{-\mathrm{Im}(\omega)t}. \tag{4-13}$$

With a characteristic time τ based on a single cycle, $\tau = (2\pi)/\mathrm{Re}(\omega)$, for the *lowest* frequency according to Table 1, the reduction of the amplitude of the optical branches becomes

$$\frac{\|\boldsymbol{U}(\boldsymbol{x},\tau)\|}{\|\boldsymbol{U}(\boldsymbol{x},0)\|} = \exp\left(-\frac{16\sqrt{2}\pi(r_D\zeta)}{Q\sqrt{1+r_K}}\,\frac{1}{Rk}\right), \tag{4-14}$$

and the reduction of the amplitude of the transverse acoustical branch becomes

$$\frac{\|\boldsymbol{U}(\boldsymbol{x},\tau)\|}{\|\boldsymbol{U}(\boldsymbol{x},0)\|} = \exp\left(-\frac{4\sqrt{2}\pi(1+4r_D)\zeta}{\sqrt{1+r_K}}\,Rk\right). \tag{4-15}$$

For small wave number k, the reduction in amplitude of the optical branches is very large (the argument of the exponent is *inversely* proportional to the wave number k), contrary to that of the acoustical branches (the argument of the exponent is proportional to the wave number k). This means that the optical branches are dampened out very rapidly, and will not be observed in situations where a continuum-mechanical description is appropriate.

5. Results

The dispersion and damping characteristics, $\mathrm{Re}(\omega)$ and $\mathrm{Im}(\omega)$, respectively, that have been obtained from the solution to the quadratic eigenvalue problem (4-7), are shown for the FCC lattice and the BCC lattice. This is done for various values of the damping factor ζ, the stiffness ratio r_K and the damping ratio r_D to show the influence of these micromechanical material characteristics on the macro-scale, continuum characteristics.

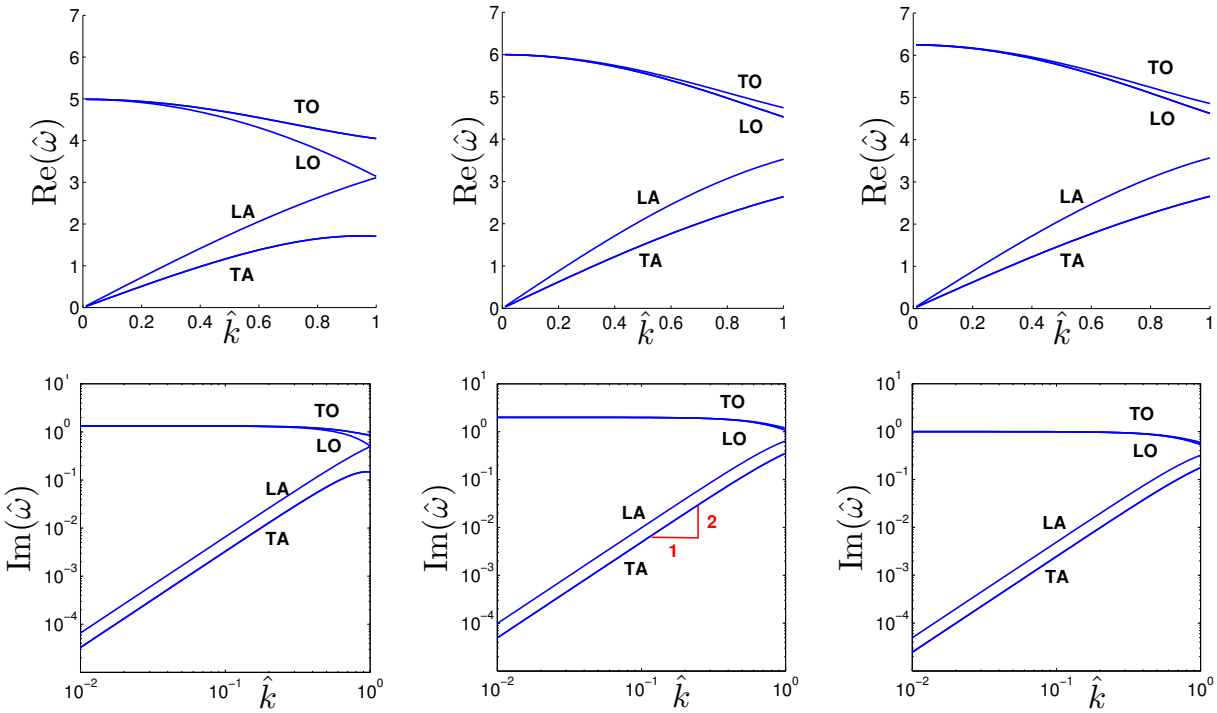

Figure 3. Dispersion characteristics (top row) and damping characteristics (bottom row). Left: BCC lattice with $\zeta = 0.05$. Middle: FCC lattice with $\zeta = 0.05$. Right: FCC lattice with $\zeta = 0.025$. In all cases $r_K = 1$; $r_D = 1$.

The middle column of Figure 3 shows typical results for the dispersion relation, Re(ω) as a function of wave number k (top graph) and for the damping characteristics Im(ω) as a function of wave number k (bottom graph).

In each of those plots four curves are shown, two acoustical branches that go through the origin and two other, optical branches. Two curves correspond to eigenfrequencies with multiplicity of one, the longitudinal branches, and two curves correspond to eigenfrequencies with multiplicity of two, the transverse branches. The total number of eigenfrequencies is six.

The two acoustical dispersion curves show an approximately linear dependence of the eigenfrequency Re(ω) on wave number k, consistent with the continuum-mechanical analysis of Section 2. The slope of the longitudinal branch is higher than that of the transverse branch. These slopes are related to the bulk modulus K and shear modulus G; see (2-6) and (2-7).

The two optical dispersion curves show a relatively weak dependence of eigenfrequency on wave number. The difference between the frequencies for the longitudinal and the transverse branches is not very large, especially for small wave numbers.

The damping characteristics of the acoustical branches show a dependence of Im(ω) on k^2, consistent with the continuum-mechanical analysis of Section 2 and with the analytical solution for the FCC lattice in Table 1. Note that the damping characteristics are presented in a log-log plot in order to show this

dependence. The damping of the optical branches is very high and is only (relatively) weakly dependent on wave number.

The results for the dispersion and the damping characteristics for the FCC lattice for small wave numbers are in agreement with the analytical expressions in Table 1.

As shown in [Suiker and de Borst 2005] for two-dimensional lattices, the direction of the wave vector $\boldsymbol{k}$ influences the dispersion relation at higher wave numbers k (small wave length), since the inherent anisotropic structure of the lattices is then apparent. For small wave number k, however, it was noted in [Suiker and de Borst 2005] that the dispersion relation is independent of the direction of the wave vector $\boldsymbol{k}$. The same is found for the three-dimensional lattices considered here (results not shown).

5A. ***Influence of lattice.*** The influence of the type of lattice on the dispersion and damping characteristics has been investigated by comparing the results for the BCC lattice (left column in Figure 3) with coordination number $Z = 8$ and for the FCC lattice (middle column) with $Z = 12$. The other micromechanical parameters are the same: $\zeta = 0.05$, $r_K = 1$ and $r_D = 1$.

Qualitatively, the dispersion and the damping characteristics for the FCC lattice and the BCC lattice are very similar. The slopes of the acoustical dispersion curves for the FCC lattice (top row, middle column in Figure 3) are larger than those for the BCC lattice (top left). This is expected, since these slopes are related to the continuum bulk and shear moduli; see Section 2. These moduli are dependent on the coordination number Z (see for example [Bathurst and Rothenburg 1988; Kruyt et al. 2010]), which is higher for the FCC lattice than for the BCC lattice. The frequency for small wave numbers of the optical branches is higher for the FCC lattice than for the BCC lattice.

The damping is higher for the FCC lattice with its higher coordination number than for the BCC lattice. A high coordination number means that a large number of contact areas (represented by the elastic springs and the viscous dashpots) is present where energy dissipation occurs.

5B. ***Influence of damping factor.*** The influence of the damping factor ζ on the dispersion and damping characteristics has been investigated by comparing the results for the FCC lattice for $\zeta = 0.05$ (middle column in Figure 3) with those for $\zeta = 0.025$ (right column). The other micromechanical parameters are the same: $r_K = 1$ and $r_D = 1$.

For small wave numbers the dispersion characteristics, $\mathrm{Re}(\omega)$, of the acoustical branches are not affected by the value of the damping factor ζ. This also follows from the analytical solution in Table 1. The frequency of the optical dispersion branches increases with decreasing damping factor ζ; see also Table 1.

As expected, a lower value of the damping factor ζ results in lower damping characteristics, $\mathrm{Im}(\omega)$, of all branches; see also Table 1.

5C. ***Influence of stiffness ratio.*** The influence of the stiffness ratio r_K on the dispersion and damping characteristics has been investigated by comparing the results with $r_K = 1$ (middle column of Figure 4) with those with $r_K = 0.5$ (left column). In this comparison the BCC lattice is considered with the other micromechanical parameters $\zeta = 0.05$ and $r_D = 1$.

For the dispersion characteristics, the slope of the acoustical branches for small wave number increases with increasing stiffness ratio r_K, since a higher value for r_K corresponds to a higher value for the shear modulus; the bulk modulus is only weakly affected by the value of the stiffness ratio when the

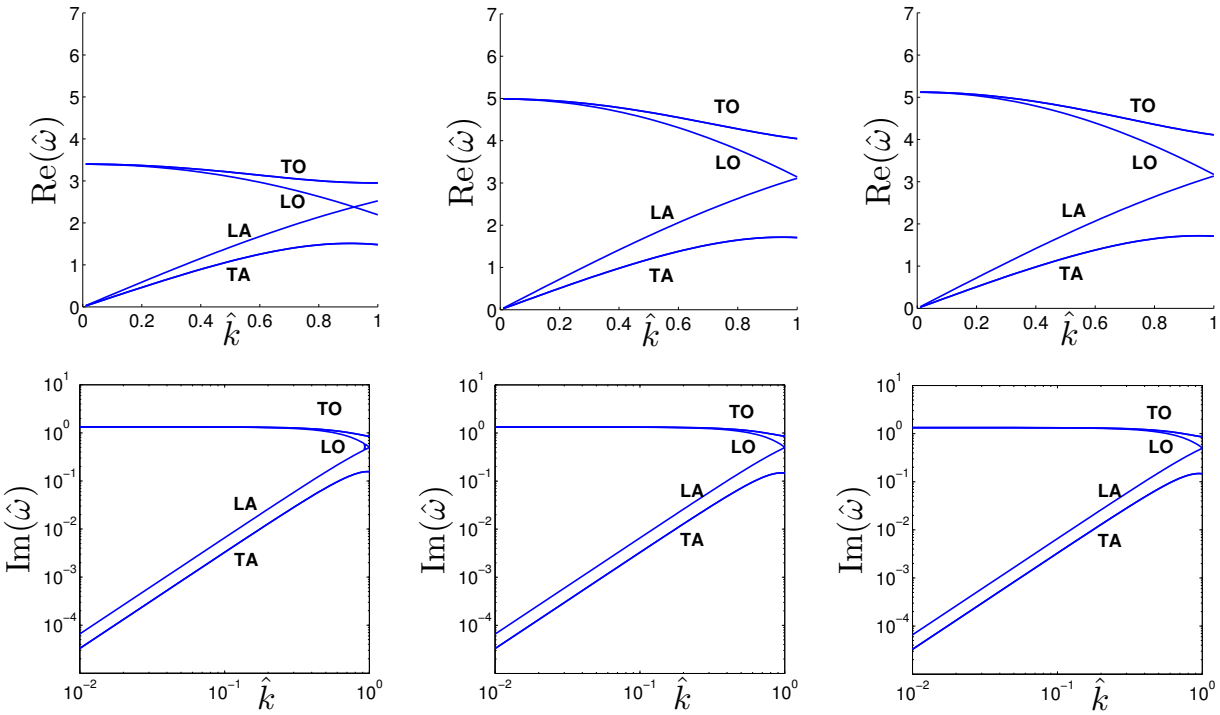

Figure 4. Dispersion characteristics (top row) and damping characteristics (bottom row). Left: $r_K = 0.5$, $r_D = 1$. Middle: $r_K = 1$, $r_D = 1$. Right: $r_K = 1$, $r_D = 0.5$. In all cases the BCC lattice is considered, with $\zeta = 0.05$.

coordination number is not low. See [Bathurst and Rothenburg 1988; Kruyt et al. 2010]. The optical branches show a higher frequency for a higher stiffness ratio. These trends for the BCC lattice are the same as for the FCC lattice; see the analytical solution in Table 1.

The damping characteristics are hardly affected by the value of the stiffness ratio. This trend is also shown by the analytical solution for the FCC lattice; see Table 1.

5D. ***Influence of damping ratio.*** The influence of the damping ratio r_D on the dispersion and damping characteristics has been investigated by comparing the results with $r_D = 1$ (middle column of Figure 4) with those with $r_D = 0.5$ (right column). In this comparison the BCC lattice is considered with the micromechanical parameters $\zeta = 0.05$ and $r_K = 1$.

The dispersion characteristics are hardly affected by the value of the damping ratio r_D. Only a small increase in the frequency of the optical branch is observed for the lower value of the damping ratio.

The damping characteristics are directly affected by the value of the damping ratio. A higher value of the damping ratio r_D gives higher damping characteristics.

These observations on the dispersion and the damping characteristics for the BCC lattice correspond to the analytical results for the FCC lattice; see Table 1.

6. Conclusions

Dispersion and damping characteristics of granular materials have been studied using a three-dimensional lattice-based approach in which the particle interaction is modeled with linear elastic springs and linear viscous dashpots. The lattice analysis leads to a quadratic eigenvalue problem for the complex eigenfrequencies.

The analysis yields acoustical and optical branches, as noted in previous studies [Schwartz et al. 1984; Suiker et al. 2001; Suiker and de Borst 2005; Kruyt 2010]. The present analysis allows for a study of the influence of the micromechanical characteristics on the continuum-mechanical dispersion and damping characteristics:

- The effect of the *type of lattice* is primarily through the coordination number. A high coordination number gives high bulk and shear moduli, and thus large slopes of the dispersion characteristics of the acoustical branches. Similarly, a high coordination number results in high damping.
- The *damping factor* has only a small effect on the dispersion characteristics of the acoustical branches. The damping increases with increasing damping factor.
- A high value of the *stiffness ratio* results in high bulk and shear moduli, and thus large slopes of the dispersion characteristics of the acoustical branches. The influence on the damping characteristics is small.
- A high value of the *damping ratio* does not affect the dispersion characteristics of the acoustical branches. A high damping ratio leads to high damping.

An important result is that the damping of the optical branches is very high. Therefore it is expected that these branches will not be observed under conditions where a continuum-mechanical description is appropriate.

The present lattice-based analysis is effectively based on the uniform-strain assumption (or mean-field assumption) for the relative displacement at contacts; see (1-1). It is well-known (see for instance [Makse et al. 1999; Kruyt and Rothenburg 2001; Kruyt and Rothenburg 2002; Kruyt et al. 2010]) that this assumption leads to an inaccurate prediction of the elastic moduli in the static case for *random* packings, especially for lower coordination numbers. It is expected that the dispersion and damping characteristics of a random packing agree qualitatively with the present results for lattices, but may show quantitative discrepancies. The quantitative study of these characteristics of random packings is a subject of further investigation.

References

[Agnolin and Roux 2007] I. Agnolin and J.-N. Roux, "Internal states of model isotropic granular packings, III: Elastic properties", *Phys. Rev. E* (3) **76**:6 (2007), 061304, 22.

[Ashcroft and Mermin 1976] N. W. Ashcroft and N. D. Mermin, *Solid state physics*, Saunders College Publishing, Fort Worth, TX, 1976.

[Bathurst and Rothenburg 1988] R. J. Bathurst and L. Rothenburg, "Micromechanical aspects of isotropic granular assemblies with linear contact interactions", *J. Appl. Mech.* (*ASME*) **55** (1988), 17–23.

[Dekker 1962] A. J. Dekker, *Solid state physics*, Macmillan, London, 1962.

[Els 2011] D. N. J. Els, "Damping of rotating beams with particle dampers: experimental analysis", *AIAA J.* **49** (2011).

[Eringen 1999] A. C. Eringen, *Microcontinuum field theories, I: Foundations and solids*, Springer, New York, 1999.

[Goddard 1990] J. D. Goddard, "Nonlinear elasticity and pressure-dependent wave speeds in granular media", *Proc. R. Soc. Lond. A* **430** (1990), 105–131.

[Horne 1965] M. R. Horne, "The behaviour of an assembly of rotound, rigid, cohesionless particles, I and II", *Proc. R. Soc. Lond. A* **286** (1965), 62–97.

[Jia et al. 1999] X. Jia, C. Caroli, and B. Velicky, "Ultrasound propagation in externally stressed granular media", *Phys. Rev. Lett.* **82** (1999), 1863–1866.

[Johnson 1985] K. L. Johnson, *Contact mechanics*, Cambridge University Press, Cambridge, UK, 1985.

[Kittel 1953] C. Kittel, *Introduction to solid state physics*, Wiley, New York, 1953.

[Kruggel-Emden et al. 2007] H. Kruggel-Emden, E. Simsek, S. Rickelt, S. Wirtz, and V. Scherer, "Review and extension of normal force models for the Discrete Element Method", *Powder Technol.* **171** (2007), 157–173.

[Kruyt 2010] N. P. Kruyt, "Three-dimensional lattice-based dispersion relations for granular materials", pp. 405–415 in *IUTAM-ISIMM Symposium on Mathematical Modelling and Physical Instances of Granular Flows, AIP Conference Proceedings*, vol. 1227, edited by J. D. Goddard et al., 2010.

[Kruyt and Rothenburg 2001] N. P. Kruyt and L. Rothenburg, "Statistics of the elastic behaviour of granular materials", *Int. J. Solids Struct.* **38** (2001), 4879–4899.

[Kruyt and Rothenburg 2002] N. P. Kruyt and L. Rothenburg, "Micromechanical bounds for the elastic moduli of granular materials", *Int. J. Solids Struct.* **39** (2002), 311–324.

[Kruyt et al. 2010] N. P. Kruyt, I. Agnolin, S. Luding, and L. Rothenburg, "Micromechanical study of elastic moduli of loose granular materials", *J. Mech. Phys. Solids* **58**:9 (2010), 1286–1301.

[Kunin 1982] I. A. Kunin, *Elastic media with microstructure, I: One-dimensional models*, Springer Series in Solid-State Sciences **26**, Springer, Berlin, 1982.

[Kunin 1983] I. A. Kunin, *Elastic media with microstructure, II: Three-dimensional models*, Springer Series in Solid-State Sciences **44**, Springer, Berlin, 1983.

[Magnanimo et al. 2008] V. Magnanimo, L. La Ragione, J. T. Jenkins, P. Wang, and H. A. Makse, "Characterizing the shear and bulk moduli of an idealized granular material", *European Physics Letters* **81** (2008). 34006.

[Makse et al. 1999] H. A. Makse, N. Gland, D. L. Johnson, and L. M. Schwartz, "Why effective medium theory fails in granular materials", *Phys. Rev. Lett.* **83** (1999), 5070–5073.

[Makse et al. 2004] H. A. Makse, N. Gland, D. L. Johnson, and L. Schwartz, "Granular packings: nonlinear elasticity, sound propagation, and collective relaxation dynamics", *Phys. Rev. E* **70** (2004), 061302.

[Mindlin 1972] R. D. Mindlin, "Elasticity, piezoelectricity and crystal lattice dynamics", *J. Elasticity* **2** (1972), 217–282.

[Mouraille 2009] O. J. P. Mouraille, *Sound propagation in dry granular materials: discrete element simulations, theory, and experiments*, Ph.D. thesis, Department of Mechanical Engineering, University of Twente, Enschede, The Netherlands, 2009.

[Myers 1997] H. P. Myers, *Introductory solid state physics*, Taylor & Francis, London, 1997.

[O'Sullivan 2011] O'Sullivan, *Particulate discrete element modelling: a geomechanics perspective*, Spon Press, London, 2011.

[Schwager and Pöschel 2007] T. Schwager and T. Pöschel, "Coefficient of restitution and linear-dashpot model revisited", *Granular Matter* **9** (2007), 465–469.

[Schwager et al. 2008] T. Schwager, V. Becker, and T. Pöschel, "Coefficient of tangential restitution for visco-elastic spheres", *Eur. Phys. J. E* **27** (2008), 107–114.

[Schwartz et al. 1984] L. M. Schwartz, D. L. Johnson, and S. Feng, "Vibrational modes in granular materials", *Phys. Rev. Lett.* **52** (1984), 831–834.

[Suiker and de Borst 2005] A. S. J. Suiker and R. de Borst, "Enhanced continua and discrete lattices for modelling granular assemblies", *Philos. Trans. R. Soc. Lond. A* **363**:1836 (2005), 2543–2580.

[Suiker et al. 2001] A. S. J. Suiker, A. V. Metrikine, and R. de Borst, "Comparison of wave propagation characteristics of the Cosserat continuum model and corresponding discrete lattice models", *Int. J. Solids Struct.* **38** (2001), 1563–1583.

[Tisseur and Meerbergen 2001] F. Tisseur and K. Meerbergen, "The quadratic eigenvalue problem", *SIAM Rev.* **43**:2 (2001), 235–286.

[Wu et al. 2003] C. Y. Wu, C. Thornton, and L. Y. Li, "Coefficients of restitution for elasto-plastic oblique impacts", *Adv. Powder Tech.* **14** (2003), 435–448.

Received 10 Oct 2011. Revised 23 Jan 2012. Accepted 7 Feb 2012.

NIELS P. KRUYT: n.p.kruyt@utwente.nl
Department of Mechanical Engineering, University of Twente, P.O. Box 217, 7500 AE Enschede, Netherlands

JOURNAL OF MECHANICS OF MATERIALS AND STRUCTURES

jomms.net

Founded by Charles R. Steele and Marie-Louise Steele

See http://jomms.net for submission guidelines.

JoMMS (ISSN 1559-3959) is published in 10 issues a year. The subscription price for 2012 is US $555/year for the electronic version, and $735/year (+$60 shipping outside the US) for print and electronic. Subscriptions, requests for back issues, and changes of address should be sent to Mathematical Sciences Publishers, Department of Mathematics, University of California, Berkeley, CA 94720–3840.

JoMMS peer-review and production is managed by EditFLOW® from Mathematical Sciences Publishers.

PUBLISHED BY

mathematical sciences publishers

http://msp.org/

A NON-PROFIT CORPORATION

Typeset in LaTeX

Journal of Mechanics of Materials and Structures

Volume 7, No. 4 April 2012